Motility-Induced Crystallization and Rotating Crystallites

Max Philipp Holl,[1,2,3,*,†] Alina Barbara Steinberg,[3,*,‡] Michael te Vrugt,[4,§] and Uwe Thiele[3,5,‖]

[1]Department of Chemistry and Materials Science, Aalto University, P.O. Box 16100, FI-00076 Aalto, Espoo 00076, Finland
[2]Academy of Finland Center of Excellence in Life-Inspired Hybrid Materials (LIBER), Aalto University, P.O. Box 16100, FI-00076 Aalto, Espoo 00076, Finland
[3]Institute of Theoretical Physics, University of Münster, Wilhelm-Klemm-Strasse 9, 48149 Münster, Germany
[4]Institute of Physics, Johannes Gutenberg University Mainz, 55128 Mainz, Germany
[5]Center for Nonlinear Science (CeNoS), University of Münster, Corrensstrasse 2, 48149 Münster, Germany

(Received 14 August 2024; revised 28 July 2025; accepted 8 September 2025; published 6 October 2025)

Active soft matter frequently shows motility-induced phase separation, where self-propelled particles condensate into clusters with an inner liquidlike structure. Such activity may also result in motility-induced crystallization into clusters with an inner crystalline structure. We derive a higher-order active phase-field-crystal model and employ it to study the interplay of passive (i.e., thermodynamic) and active (i.e., motility-induced) condensation or evaporation and crystallization or melting. Stability and morphological phase diagrams indicate the various occurring phase coexistences and transitions, e.g., the destruction of passive clusters in the case of a density-independent effective velocity and the possible creation of active clusters in the case of a density-dependent effective velocity. Finally, simple and complex rotating crystallites are discussed, including states of time-periodic chirality.

DOI: 10.1103/m3dy-53yc

Motility-induced phase separation (MIPS) is an important focus of attention in the physics of active soft matter: when the driving activity of self-propelled particles crosses a critical density-dependent threshold the particles phase-separate into dense and dilute fluid phases even in the absence of attractive interactions. In other words they accumulate into high-density liquidlike clusters that coexist with a low-density gaslike phase [1–7]. Experimental observations [3,8–10], particle-based simulations [11–17], and continuum models mainly based on nonvariational amendments [18–23] of the Cahn-Hilliard model for phase decomposition [24] all yield consistent results for the existence and properties of such clusters [22]. Furthermore, motility can also strongly amend the phase behavior for systems that have rich phase diagrams already in the passive limit. For instance, in motility-enhanced (motility-suppressed) phase separation the parameter range where phase separation occurs is enlarged (reduced).

*These authors contributed equally to this work.
†Contact author: max.holl@aalto.fi
‡Contact author: a_stei52@uni-muenster.de
§Contact author: tevrugtm@uni-mainz.de
‖Contact author: u.thiele@uni-muenster.de; www.uwethiele.de

Published by the American Physical Society under the terms of the Creative Commons Attribution 4.0 International license. Further distribution of this work must maintain attribution to the author(s) and the published article's title, journal citation, and DOI.

However, besides the clusters of liquidlike inner structure that result from phase separation, experiments and simulations also increasingly report the existence of active (or "living") crystallites, i.e., resting, traveling, or rotating particle clusters with an inner crystalline structure [8,9,12,25–30] that represent active solids [31–34] of finite size. Frequently, their dynamics is investigated using active phase-field-crystal (active PFC) models [35–43], i.e., active equivalents of the passive PFC model 46–44]]—a versatile microscopic field theory for colloidal crystallization that itself is a local approximation of a dynamical density functional theory (DDFT) [47,48] and has the form of a conserved Swift-Hohenberg equation [46]. Such models are well suited to investigate activity-induced (nonequilibrium) phase transitions, multistability, time-periodic states, etc.

Although the standard active PFC model well captures the transition from resting to traveling space-filling crystalline states [35], and also predicts the existence of active crystallites in the form of resting and traveling localized states [39,42,43] it suffers from two major shortcomings: First, in the passive limit, it only describes the fluid-solid phase behavior for a single fluid phase (that is normally interpreted as liquid), but fails to capture the liquid-gas transition. Therefore, the model cannot be employed to study the interplay of condensation and crystallization. Second, it does not describe proper *motility-induced crystallization* (MIC) where activity induces crystallization. Instead, with the standard active PFC model an increase in activity tends to destroy preexisting crystalline

states [35,41,42]. In other words, the crystallization of passive (i.e., thermodynamic) crystalline clusters described by a passive PFC model [46,49] is subdued by incorporating activity that also results in the transition from resting to moving (and oscillating) crystals [41].

Here, we present a microscopically derived extended active PFC model that mitigates both shortcomings: On the one hand, in the appropriate limit it corresponds to the passive higher-order PFC model of Wang *et al.* [50] that faithfully captures phase transitions between all three phases: the liquid-gas transition between low- and high-density uniform phases as well as liquid-solid and gas-solid transitions between uniform (gas or solid) and spatially periodic (crystalline) phases. In consequence, it captures the basic phase diagram featuring gas, liquid, and solid phases including gas-liquid-solid coexistence, as well as all corresponding dynamic transitions. In contrast to the standard PFC model [44–48] its underlying free energy functional $\mathcal{F}_{\mathrm{PFC}}[\phi]$ includes contributions from three- and four-point direct correlation functions and contains derivatives of up to sixth order. A typical phase diagram in the vicinity of the triple point (three-phase coexistence) is given in Fig. 2(a) below.

On the other hand, our derivation extends the approach of [35,36] regarding activity resulting from self-propulsion. In particular, our model not only features a density-independent effective velocity [35], but additionally a microscopically justified density-dependent contribution similar to a classical MIPS model [51]. This enables our model to describe both—the destruction of passive clusters and the creation of active ones as schematically illustrated in Fig. 1. In the following, we briefly present the model, analyze its phase behavior focusing on the destruction of passive (thermodynamic) clusters, i.e., drops and crystallites, and the emergence of active ones. Finally, we analyze the emerging rotating crystallites and point out intriguing states with complex chirality dynamics.

Overall, the passive dynamics of the amended PFC model [50] in terms of the conserved density field $\phi(\mathbf{x}, t)$ is nonvariationally coupled to the dynamics of a polarization field $\mathbf{P}$ that indicates the local strength and direction of polar order related to the drive of the active particles. The resulting dynamic model is

$$\partial_t \phi = \nabla^2 \frac{\delta \mathcal{F}[\phi, \mathbf{P}]}{\delta \phi} - \nabla \cdot [v(\phi)\mathbf{P}], \tag{1}$$

$$\partial_t \mathbf{P} = \nabla^2 \frac{\delta \mathcal{F}[\phi, \mathbf{P}]}{\delta \mathbf{P}} - D_r \frac{\delta \mathcal{F}[\phi, \mathbf{P}]}{\delta \mathbf{P}} - \nabla[\alpha v(\phi)(\phi + \rho_r)]. \tag{2}$$

Note that ϕ and temperature T are nondimensional scaled and shifted effective quantities (ρ_r is a reference density) as further detailed in Sec. A of the Supplemental Material [52], where also the full expression for the density- and polarization-dependent energy $\mathcal{F}[\phi, \mathbf{P}] = \mathcal{F}_{\mathrm{PFC}}[\phi] + \mathcal{F}_{\mathbf{P}}[\mathbf{P}]$ is given, including the dependence on T. The first and second term on the right-hand side of Eq. (2) correspond to translational and rotational diffusion, respectively. Besides these terms that represent respective conserved and nonconserved gradient dynamics, there are the active coupling terms [the respective final term of Eqs. (1) and (2)] [73]. Their nonreciprocal character breaks the overall gradient dynamics structure, i.e., represents sustained nonequilibrium influences like chemomechanical driving. They are ultimately responsible for all occurring moving and oscillating states.

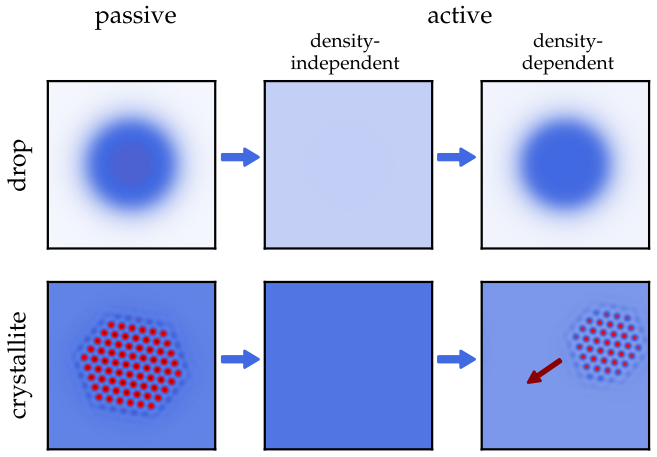


FIG. 1. A schematic illustration of the destruction of passive (thermodynamic) drops (top) and crystallites (bottom) by an increase of activity from zero (left to center), and the subsequent re-creation of both cluster types by increasing a density-dependent velocity.

The strength $v(\phi)$ of the coupling between the density and polarization represents the effective self-propulsion speed of the active particles that is often assumed constant [35,39]. In contrast, here, we have obtained the density-dependent expression $v(\phi) = v_0 - \zeta(\phi + \rho_r)$ that is widely used in effective hydrodynamic models for MIPS [19,20,23,51]. Thereby, v_0 represents an effective speed of an individual self-propelled particle while ζ results from the force imbalance related to the self-trapping due to interactions with other particles as frequently occurring at larger densities. Note that more complicated expressions [e.g., $v(\phi, \nabla^2\phi)$] may also be employed [21,23,74] but do not amend our central result. A derivation from a microscopic DDFT and a discussion of the quantitative relation to classical MIPS models [51] are provided in Secs. B and D of Supplemental Material [52], respectively.

The higher-order active PFC model (1) and (2) shows the range of behaviors sketched in Fig. 1: In the passive case ($v = 0$) the full phase behavior of a system with gas, liquid, and crystalline state is reproduced [50], shown here in Fig. 2(a) by a phase diagram in the plane spanned by effective mean density $\bar{\phi}$ and temperature T with a focus on the vicinity of the triple point at $(\bar{\phi}, T) \approx (-0.5, 0)$.

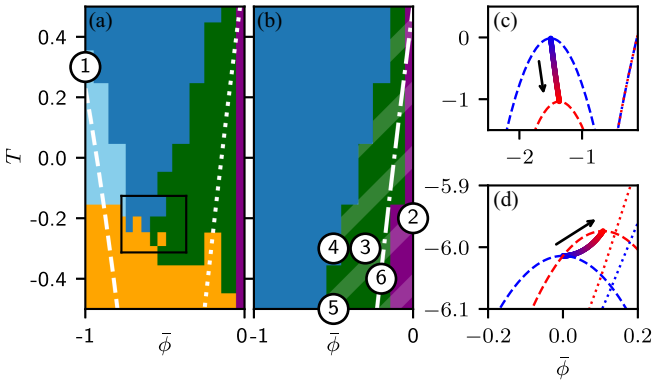


FIG. 2. Morphological phase diagrams for the extended PFC model (1) and (2) in the plane spanned by effective mean density $\bar{\phi}$ and temperature T. Shown are (a) the passive case ($v = 0$) and (b) an active case ($v_0 = 1, \zeta = 0$) with a focus on the vicinity of the triple point in the passive case [at $(\bar{\phi}, T) \approx (-0.5, 0)$] for the parameters of Ref. [50]. Time simulations are employed for finite domain size $L_x \times L_y = 100 \times 100$. Examples of occurring states at numbered loci ①-⑥ are given in Fig. 3. Dark blue indicates uniform states (gas or liquid), while light blue marks liquid-gas coexistence. Green and orange represent coexistence of a crystalline phase with liquid and gas state, respectively. The latter may also include finite-size realizations of three-phase coexistence. Finally, dark purple indicates domain-filling crystalline states. In (a) all states are at rest while in (b) moving states are shown hatched. The white dashed and dotted lines give linear stability thresholds for a Cahn-Hilliard and a conserved-Turing instability related to spinodals for phase separation and crystallization, respectively. The dot-dashed line in (b) indicates a conserved-wave instability related to the direct crystallization into moving crystals. The full set of parameters is given in Sec. A of Supplemental Material [52]. The employed parameter increments for $\bar{\phi}$ and T are both 0.1 [0.05 within the square in (a)]. Finally, panels (c) and (d) show how the spinodals change with increasing $\zeta \geq 0$ (indicated by arrows) in two qualitatively different cases. In each case, blue [red] lines indicate $\zeta = 0[\zeta > 0]$. Specifically, (c) $v_0 = 1, \zeta = 0.2$, (d) $v_0 = 0.5$, $\zeta = 0.5$. The colored dots show the trace of the liquid-gas critical point. Specifically, in (c) ζ further suppresses phase separation for otherwise identical parameters as in (a),(b), while in (d) ζ enhances both, phase separation and crystallization (also see Sec. C of Supplemental Material [52], for remaining parameters see Table 1 of [52]).

For details on the employed time simulations see Sec. E of [52]. There is a one-phase region of uniform states (dark blue, liquid or gas), and two-phase regions of liquid-gas (light blue), solid-liquid (dark green), and solid-gas coexistence (orange). The white lines indicate linear stability thresholds for the uniform state, i.e., spinodals, with respect to liquid-gas phase separation (dashed) and crystallization (dotted). They correspond to Cahn-Hilliard (stationary, large-scale) and conserved-Turing instabilities (stationary, small-scale), respectively (see classification of Ref. [75]). Typical dispersion relations and complete spinodals are given in Sec. C of Supplemental Material [52].

Increasing the density-independent velocity v_0 (at $\zeta = 0$) from zero significantly changes the phase diagram [see Fig. 2(b)]. Overall, all clustering is reduced, the region of liquid-gas phase separation has disappeared from the shown region and crystallization is shifted toward larger densities. The dot-dashed spinodal now indicates the onset of a conserved-wave instability [75] related to the direct emergence of traveling crystalline states. The shift is consistent with the suppression of crystallization with increasing activity observed in the standard active PFC model [35,39,41]. Here, it applies as well to phase separation where with increasing v_0 the liquid-gas critical point and the spinodals are shifted toward lower temperatures. One further deduces from Fig. 2(b) that crystal-gas coexistence [yellow in Fig. 2(a)] has also shifted to similarly low values, as indicated by states ⑦ and ⑧ in Fig. 3. The remaining crystalline states all correspond to traveling states, see examples in Fig. 3. Thereby, finite-size crystallites corresponding to crystal-liquid coexistence frequently rotate as further analyzed below (also translational motion may occur). In summary, pre-existing structures that result from passive forces, i.e., by thermodynamic interactions between particles, are all counteracted by the density-independent velocity v_0.

Then, in the hatched purple region domain-filling stationary traveling crystals are found (state ①). Coexistence of drops with an extended traveling crystal has emerged (states ⑤ and ⑥). Finally, ⑦ and ⑧ provide examples of three-phase gas-liquid-solid coexistence in an active system, in the former note the liquid wetting layer at the crystal-gas interface. Note that coexisting states may also exist outside the spinodally unstable region, i.e., the borders between the colored regions in Fig. 2 represent finite-size approximations of (non)equilibrium binodals. This indicates that all transitions are of first order as also confirmed by the existence of various localized states [43,46,76]. A detailed understanding of the intricate relations between and multistability of the various uniform, periodic and localized states (that may rest or move), in particular, in the vicinity of the triple point can be achieved by considering the bifurcation structure for finite systems. A selection of corresponding results is given in Sec. F of Supplemental Material [52]. Note that in contrast to most results described for the standard active PFC model [35,39,41], here, the group velocity of the crystallites is lower than their phase velocity, i.e., individual peaks move faster than the overall structure (states ④, ⑥ to ⑧ in Fig. 3). Physically, this corresponds to particles melting at the front of the traveling crystallite into the coexisting uniform phase and crystallizing at the rear. In other words, at the rear particles get stuck in the "slowly moving traffic jam" of the crystallite, then slowly move through it until they detach themselves when reaching the front.

Interestingly, an additional density-dependent velocity of strength ζ can either further suppress clustering [see Fig. 2(c)

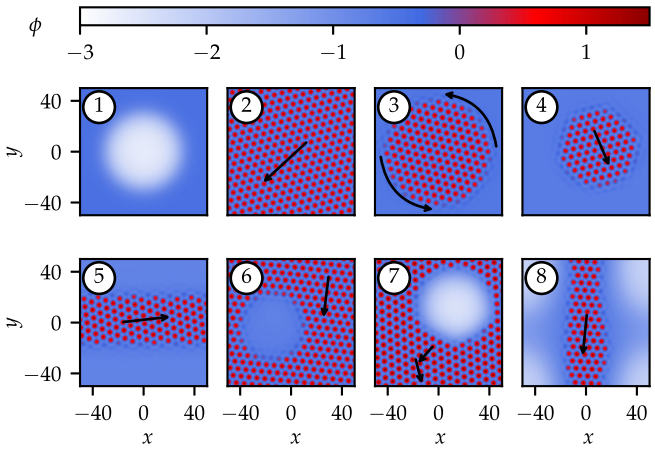


FIG. 3. Typical snapshots of various resting and moving states are represented by their density profiles $\phi(\mathbf{x}, t)$. Panels ① to ⑥ show states at parameter values indicated by corresponding numbers in Figs. 2(a) and 2(b). ⑦ and ⑧ give states with $v_0 = 1$ at $(\bar{\phi}, T) = (-0.5, -0.8)$ and $(-1, -0.58)$, respectively. Given are ① a phase-separated state of a gas bubble inside a liquid, ② an extended traveling crystal, ③ to ⑧ various types of moving crystallites. The black arrows indicate the direction of motion of the crystalline regions. Three-phase coexistence is visible in ⑦ and ⑧. A movie can be found in Supplemental Material [52].

for otherwise identical parameters as in Figs. 2(a) and 2(b)] or foster the creation of active clusters [Fig. 2(d)], also cf. Fig. 7 of Supplemental Material [52]. In the latter case an increase in ζ enhances both, phase separation and crystallization. In particular, the liquid-gas spinodal is moving to higher temperatures and densities while the liquid-crystal binodal moves to lower densities. The resulting transitions one may call MIPS and MIC. Note that in the corresponding density range our model quantitatively reproduces corresponding literature results for MIPS obtained with simpler models that do not account for crystallization as well as results for an active Cahn-Hilliard model. This is detailed in Sec. C of [52]. Note that in the case of Fig. 2(d) the resulting small distance between the critical and triple point implies that crystallites nonlinearly dominate even in part of the phase-separation region.

An intriguing state are rotating crystallites as state ③ in Fig. 3. Such states are described for many experimental systems [27,32,77–80] and particle-based simulations [15,81], both for chiral [29,78,81] and nonchiral [15,32,82,83] particles. However, such states are rarely mentioned in studies employing PFC models ([38] shows their existence for a circular domain). Here, they frequently occur beside the also found traveling crystallites (state ④ in Fig. 3). On general grounds, both should be expected even for nonchiral particles as the corresponding collective motions result from the interaction of pitchfork bifurcations with Goldstone modes related to homogeneity and isotropy of space, respectively. Such drift- and rotation-pitchfork bifurcations were studied e.g., for a reaction-diffusion system [84].

Here, the simplest rotating crystalline clusters move as a nearly hexagonal rigid body, i.e., with identical group and phase velocity. Figure 4 provides an overview of their characteristics. Their radius R and angular velocity ω are given as a function of T and R, respectively, at several fixed densities $\bar{\phi} = -0.2\ldots -0.45$. The dependence $R(T)$ has the appearance of a staircase that goes up with decreasing T while the steps are getting longer (at equal height), a typical behavior for localized states that show homoclinic snaking [85,86]. Figure 4 focuses on localized states with a central peak, though states with a central hole also exist and show a similar stairlike behavior. Inspecting profiles like Figs. 4(c) and 4(d) shows that along each of the nearly horizontal parts an initially incomplete outer shell of the hexagonal structure laterally grows more peaks with decreasing T. When a shell is completed, a new outer layer is initiated by peaks in the central part of each face that then grows, thereby resulting in the steplike increase of R. In other words, each step corresponds to a stable radius. A corresponding structure is visible in the dependence of ω on R [Fig. 4(b)] where for small clusters the velocity decreases with increasing cluster size while at large R one can discern a very small increase. Beside the shown clusters of overall sixfold symmetry, also less symmetric states exist that feature facets of different lengths (not shown). Further note that for the employed domain size, clusters above $R_{\max} \approx 45.3$ interact via the boundaries, ultimately form other states, and are therefore excluded from the analysis. Similarly, there is a minimal radius $R_{\min} \approx 13.7$ corresponding to the smallest stable cluster (two layers around the central peak). Lower densities result in uniform states [87].

At more extreme conditions, e.g., lower temperature and larger density with $\zeta > 0$ and $\rho_r = 3$ more intricate behavior is observed: There, also a stripe phase exists (as in standard PFC models [35,46]) that corresponds to particles that are periodically placed in one direction but are mobile in the other one. This results in the new types of localized states shown in Fig. 5. They are often of lower symmetry and either combine local stripe and crystalline arrangements [two-phase cluster, Figs. 5(c)–5(g)] or predominantly consist of localized stripe phase [Figs. 5(b) and 5(h)]. Because of the activity the entire clusters and their parts may move in different ways. A recurring type of movement is the swinging motion found in Figs. 5(a), 5(b), and 5(e). Such a pattern of time-periodic chirality is reminiscent of a torsion pendulum and implies a periodic reversal in the polarization field. It can also be found in experiments, e.g., see Ref. [77]. Other motion types which mostly involve the stripe phase resemble bouncing [Fig. 5(c)], waving [Figs. 5(b) and (5e)] and wobbling [Figs. 5(c)–5(e) and 5(g)], see movie in Supplemental Material [52]. In experiments or simulations such states

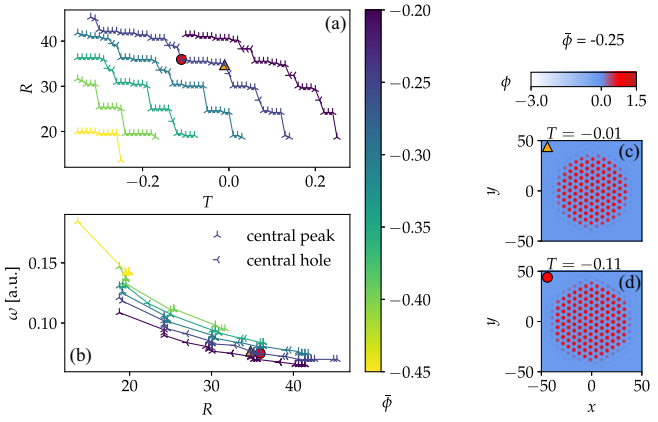


FIG. 4. Characteristics of rotating crystallites for the case of $v_0 = 1$ and $\zeta = 0$. Shown are (a) the radius R in dependence of the temperature T and (b) the angular velocity ω (in degree per time unit) as a function of R, both at several fixed mean densities $\bar{\phi}$ as indicated by the color bar. Panels (c) and (d) show profiles of states at the two ends of a single plateau at $\bar{\phi} = -0.25$ in (a) where they are marked by an orange triangle and red circle, respectively. The domain size is $L_x = L_y = 100$, for numerical details see Sec. E of Supplemental Material [52].

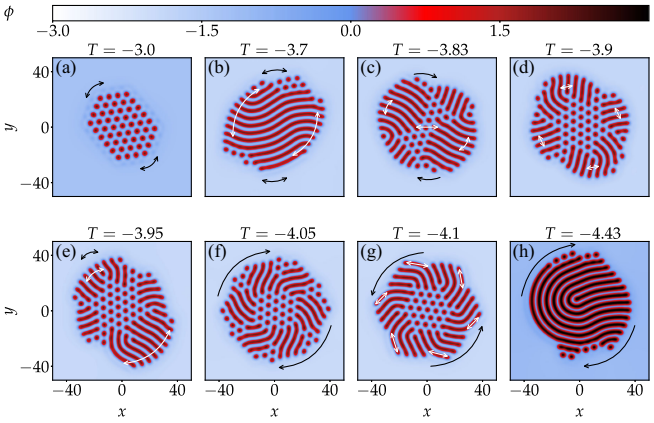


FIG. 5. Intricate chiral behavior of active crystalline clusters at $\bar{\phi} = -1$ and rather low T (as given at the panels). Black and white arrows indicate main overall and inner modi of motion, respectively, and ϕ is given by the color bar. The individual states are described in the main text and Supplemental Material [52] where also a movie is given. Remaining parameters are $\zeta = 1$ and $\rho_r = 3$.

would correspond to clusters with a rigid core structure and a less rigid but still crystalline outer part. Figure 4(b) of [80] shows some promising candidates. There, time traces visualize particle motion, i.e., their large lower left cluster combines strongly and weakly moving particles in the same crystallite, suggesting that some of them are stronger bound to their position than others, and further clusters show wavy time traces. This suggests modes of relative motion as seen in our Fig. 5.

To conclude, we have presented an amended active phase-field-crystal model capable of describing (active) gas, liquid and solid phases, including their dynamics in the vicinity of the triple point. This has allowed us to study the interplay of passive and active condensation and crystallization including phase coexistences. This includes a variety of traveling and rotating crystallites, i.e., finite-size active solids, that may coexist with gas or liquid as further evidenced by phase diagrams and a detailed study of rotating crystallites. States with time-periodic chirality, i.e., direction-reversing rotational waves, have also been described.

Phase diagrams obtained with the present continuum approach qualitatively match results of particle-based simulations, see, e.g., Refs. [16,17] (when accounting for their nondimensionalization), even though their models are for hard spheres [88]. Studies with softer attractive particles should identify the destruction of passive clusters and creation of active ones as well in particle-based simulations and experiments. Incorporating the approach of [89], the model may also be extended toward spinning particles with resulting effective interactions [78]. Finally, note that the presented conceptually relatively simple continuum model may be adapted to study many effects that involve active solid, liquid, and gas phase as phenomena of nonequilibrium pattern formation. Examples include wetting phenomena on active solids, nucleation processes for active crystals and premelting transitions at grain boundaries of active solids.

Acknowledgments—We acknowledge usage of the HPC cluster PALMA II of the University of Münster, subsidized by the DFG (No. INST 211/667-1). M. t. V. is funded by the Deutsche Forschungsgemeinschaft (DFG, German Research Foundation)—SFB 1551, Project-ID 464588647.

Data availability—The data that support the findings of this article are openly available [90].

[1] S. Ramaswamy, The mechanics and statistics of active matter, Annu. Rev. Condens. Matter Phys. **1**, 323 (2010).
[2] P. Romanczuk, M. Bär, W. Ebeling, B. Lindner, and L. Schimansky-Geier, Active Brownian particles from individual to collective stochastic dynamics, Eur. Phys. J. Spec. Top. **202**, 1 (2012).
[3] M. C. Marchetti, J. F. Joanny, S. Ramaswamy, T. B. Liverpool, J. Prost, M. Rao, and R. A. Simha, Hydrodynamics of soft active matter, Rev. Mod. Phys. **85**, 1143 (2013).
[4] M. E. Cates and J. Tailleur, Motility-induced phase separation, Annu. Rev. Condens. Matter Phys. **6**, 219 (2015).
[5] D. Marenduzzo, An introduction to the statistical physics of active matter: Motility-induced phase separation and the "generic instability" of active gels, Eur. Phys. J. Spec. Top. **225**, 2065 (2016).
[6] G. Gompper *et al.*, The 2020 motile active matter roadmap, J. Phys. Condens. Matter **32**, 193001 (2020).

[7] M. R. Shaebani, A. Wysocki, R. G. Winkler, G. Gompper, and H. Rieger, Computational models for active matter, Nat. Rev. Phys. **2**, 181 (2020).

[8] I. Buttinoni, J. Bialké, F. Kümmel, H. Löwen, C. Bechinger, and T. Speck, Dynamical clustering and phase separation in suspensions of self-propelled colloidal particles, Phys. Rev. Lett. **110**, 238301 (2013).

[9] C. Bechinger, R. Di Leonardo, H. Löwen, C. Reichhardt, G. Volpe, and G. Volpe, Active particles in complex and crowded environments, Rev. Mod. Phys. **88**, 045006 (2016).

[10] A. A. Fragkopoulos, J. Vachier, J. Frey, F.-M. Le Menn, M. G. Mazza, M. Wilczek, D. Zwicker, and O. Bäumchen, Self-generated oxygen gradients control collective aggregation of photosynthetic microbes, J. R. Soc. Interface **18**, 20210553 (2021).

[11] F. D. C. Farrell, M. C. Marchetti, D. Marenduzzo, and J. Tailleur, Pattern formation in self-propelled particles with density-dependent motility, Phys. Rev. Lett. **108**, 248101 (2012).

[12] B. M. Mognetti, A. Saric, S. Angioletti-Uberti, A. Cacciuto, C. Valeriani, and D. Frenkel, Living clusters and crystals from low-density suspensions of active colloids, Phys. Rev. Lett. **111**, 245702 (2013).

[13] A. Patch, D. Yllanes, and M. C. Marchetti, Kinetics of motility-induced phase separation and swim pressure, Phys. Rev. E **95**, 012601 (2017).

[14] E. Crosato, M. Prokopenko, and R. E. Spinney, Irreversibility and emergent structure in active matter, Phys. Rev. E **100**, 042613 (2019).

[15] L. Caprini, U. Marini Bettolo Marconi, and A. Puglisi, Spontaneous velocity alignment in motility-induced phase separation, Phys. Rev. Lett. **124**, 078001 (2020).

[16] F. Turci and N. B. Wilding, Phase separation and multibody effects in three-dimensional active Brownian particles, Phys. Rev. Lett. **126**, 038002 (2021).

[17] A. K. Omar, K. Klymko, T. GrandPre, and P. L. Geissler, Phase diagram of active Brownian spheres: Crystallization and the metastability of motility-induced phase separation, Phys. Rev. Lett. **126**, 188002 (2021).

[18] R. Wittkowski, A. Tiribocchi, J. Stenhammar, R. J. Allen, D. Marenduzzo, and M. E. Cates, Scalar ϕ^4 field theory for active-particle phase separation, Nat. Commun. **5**, 4351 (2014).

[19] T. Speck, J. Bialké, A. M. Menzel, and H. Löwen, Effective Cahn-Hilliard equation for the phase separation of active Brownian particles, Phys. Rev. Lett. **111**, 218304 (2014).

[20] T. Speck, A. M. Menzel, J. Bialké, and H. Löwen, Dynamical mean-field theory and weakly non-linear analysis for the phase separation of active Brownian particles, J. Chem. Phys. **142**, 224109 (2015).

[21] L. Rapp, F. Bergmann, and W. Zimmermann, Systematic extension of the Cahn-Hilliard model for motility-induced phase separation, Eur. Phys. J. E **42**, 57 (2019).

[22] J. Bickmann and R. Wittkowski, Predictive local field theory for interacting active Brownian spheres in two spatial dimensions, J. Phys. Condens. Matter **32**, 214001 (2020).

[23] J. Bickmann and R. Wittkowski, Collective dynamics of active Brownian particles in three spatial dimensions: A predictive field theory, Phys. Rev. Res. **2**, 033241 (2020).

[24] A. J. Bray, Theory of phase-ordering kinetics, Adv. Phys. **43**, 357 (1994).

[25] I. Theurkauff, C. Cottin-Bizonne, J. Palacci, C. Ybert, and L. Bocquet, Dynamic clustering in active colloidal suspensions with chemical signaling, Phys. Rev. Lett. **108**, 268303 (2012).

[26] J. Palacci, S. Sacanna, A. P. Steinberg, D. J. Pine, and P. M. Chaikin, Living crystals of light-activated colloidal surfers, Science **339**, 936 (2013).

[27] A. P. Petroff, X.-L. Wu, and A. Libchaber, Fast-moving bacteria self-organize into active two-dimensional crystals of rotating cells, Phys. Rev. Lett. **114**, 158102 (2015).

[28] A. Zöttl and H. Stark, Emergent behavior in active colloids, J. Phys. Condens. Matter **28**, 253001 (2016).

[29] A. P. Petroff and A. Libchaber, Nucleation of rotating crystals by Thiovulum majus bacteria, New J. Phys. **20**, 015007 (2018).

[30] F. Ginot, I. Theurkauff, F. Detcheverry, C. Ybert, and C. Cottin-Bizonne, Aggregation-fragmentation and individual dynamics of active clusters, Nat. Commun. **9**, 696 (2018).

[31] R. J. Hawkins and T. B. Liverpool, Stress reorganization and response in active solids, Phys. Rev. Lett. **113**, 028102 (2014).

[32] C. Hernández-López, P. Baconnier, C. Coulais, O. Dauchot, and G. Düring, Model of active solids: Rigid body motion and shape-changing mechanisms, Phys. Rev. Lett. **132**, 238303 (2024).

[33] E. Ferrante, A. E. Turgut, M. Dorigo, and C. Huepe, Elasticity-based mechanism for the collective motion of self-propelled particles with springlike interactions: A model system for natural and artificial swarms, Phys. Rev. Lett. **111**, 268302 (2013).

[34] A. Maitra and S. Ramaswamy, Oriented active solids, Phys. Rev. Lett. **123**, 238001 (2019).

[35] A. M. Menzel and H. Löwen, Traveling and resting crystals in active systems, Phys. Rev. Lett. **110**, 055702 (2013).

[36] A. M. Menzel, T. Ohta, and H. Löwen, Active crystals and their stability, Phys. Rev. E **89**, 022301 (2014).

[37] A. I. Chervanyov, H. Gomez, and U. Thiele, Effect of the orientational relaxation on the collective motion of patterns formed by self-propelled particles, Europhys. Lett. **115**, 68001 (2016).

[38] F. Alaimo, S. Praetorius, and A. Voigt, A microscopic field theoretical approach for active systems, New J. Phys. **18**, 083008 (2016).

[39] L. Ophaus, S. V. Gurevich, and U. Thiele, Resting and traveling localized states in an active phase-field-crystal model, Phys. Rev. E **98**, 022608 (2018).

[40] S. Praetorius, A. Voigt, R. Wittkowski, and H. Löwen, Active crystals on a sphere, Phys. Rev. E **97**, 052615 (2018).

[41] L. Ophaus, J. Kirchner, S. V. Gurevich, and U. Thiele, Phase-field-crystal description of active crystallites: Elastic and inelastic collisions, Chaos **30**, 123149 (2020).

[42] L. Ophaus, E. Knobloch, S. V. Gurevich, and U. Thiele, Two-dimensional localized states in an active phase-field-crystal model, Phys. Rev. E **103**, 032601 (2021).

[43] M. P. Holl, A. J. Archer, S. V. Gurevich, E. Knobloch, L. Ophaus, and U. Thiele, Localized states in passive and active phase-field-crystal models, IMA J. Appl. Math. **86**, 896 (2021).

[44] K. R. Elder, M. Katakowski, M. Haataja, and M. Grant, Modeling elasticity in crystal growth, Phys. Rev. Lett. **88**, 245701 (2002).

[45] H. Emmerich, H. Löwen, R. Wittkowski, T. Gruhn, G. I. Tóth, G. Tegze, and L. Gránásy, Phase-field-crystal models for condensed matter dynamics on atomic length and diffusive time scales: An overview, Adv. Phys. **61**, 665 (2012).

[46] U. Thiele, A. J. Archer, M. J. Robbins, H. Gomez, and E. Knobloch, Localized states in the conserved Swift-Hohenberg equation with cubic nonlinearity, Phys. Rev. E **87**, 042915 (2013).

[47] A. J. Archer, D. J. Ratliff, A. M. Rucklidge, and P. Subramanian, Deriving phase field crystal theory from dynamical density functional theory: Consequences of the approximations, Phys. Rev. E **100**, 022140 (2019).

[48] M. te Vrugt, H. Löwen, and R. Wittkowski, Classical dynamical density functional theory: From fundamentals to applications, Adv. Phys. **69**, 121 (2020).

[49] P. Subramanian, A. J. Archer, E. Knobloch, and A. M. Rucklidge, Spatially localized quasicrystalline structures, New J. Phys. **20**, 122002 (2018).

[50] Z.-L. Wang, Z. Liu, Z.-F. Huang, and W. Duan, Minimal phase-field crystal modeling of vapor-liquid-solid coexistence and transitions, Phys. Rev. Mater. **4**, 103802 (2020).

[51] J. Bialké, H. Löwen, and T. Speck, Microscopic theory for the phase separation of self-propelled repulsive disks, Europhys. Lett. **103**, 30008 (2013).

[52] See Supplemental Material at http://link.aps.org/supplemental/10.1103/m3dy-53yc for details on the underlying energy functional, governing equations and parameters, a microscopic derivation of the model, a linear stability analysis of uniform states, a discussion of the quantitative relation to classical MIPS and active Cahn-Hilliard models, details on the used numerical methods, and an analysis of the bifurcation behavior for one-dimensional states. It also includes Refs. [53–72].

[53] J. P. Boyd, *Chebyshev and Fourier Spectral Methods* (Dover Publ., Mineola, NY, 2. (rev.) edition, 2001).

[54] S. Engelnkemper, S. V. Gurevich, H. Uecker, D. Wetzel, and U. Thiele, Continuation for thin film hydrodynamics and related scalar problems, in *Computational Modeling of Bifurcations and Instabilities in Fluid Mechanics*, edited by A. Gelfgat, Computational Methods in Applied Sciences Vol. 50 (Springer, Cham, 2019), pp. 459–501, 10.1007/978-3-319-91494-7_13.

[55] H. Uecker, D. Wetzel, and J. D. M. Rademacher, PDE2PATH—a Matlab package for continuation and bifurcation in 2D elliptic systems, Numer. Math. Theory Methods Appl. **7**, 58 (2014).

[56] D. Greve and U. Thiele, An amplitude equation for the conserved-Hopf bifurcation—derivation, analysis, and assessment, Chaos **34**, 123134 (2024).

[57] G. S. Redner, M. F. Hagan, and A. Baskaran, Structure and dynamics of a phase-separating active colloidal fluid, Phys. Rev. Lett. **110**, 055701 (2013).

[58] M. te Vrugt and R. Wittkowski, Relations between angular and Cartesian orientational expansions, AIP Adv. **10**, 035106 (2020).

[59] M. te Vrugt, J. Bickmann, and R. Wittkowski, How to derive a predictive field theory for active Brownian particles: A step-by-step tutorial, J. Phys. Condens. Matter **35**, 313001 (2023).

[60] M. te Vrugt, M. P. Holl, A. Koch, R. Wittkowski, and U. Thiele, Derivation and analysis of a phase field crystal model for a mixture of active and passive particles, Modelling Simul. Mater. Sci. Eng. **30**, 084001 (2022).

[61] S. Hermann, P. Krinninger, D. de las Heras, and M. Schmidt, Phase coexistence of active Brownian particles, Phys. Rev. E **100**, 052604 (2019).

[62] Z.-F. Huang, M. te Vrugt, R. Wittkowski, and H. Löwen, Active pattern formation emergent from single-species nonreciprocity, arXiv:2404.10093.

[63] Z.-F. Huang, M. te Vrugt, R. Wittkowski, and H. Löwen, Anomalous grain dynamics and grain locomotion of odd crystals, arXiv:2505.03957 [Proc. Natl. Acad. Sci. U.S.A. (to be published)].

[64] R. Wittkowski, J. Stenhammar, and M. E. Cates, Non-equilibrium dynamics of mixtures of active and passive colloidal particles, New J. Phys. **19**, 105003 (2017).

[65] S. Bröker, M. te Vrugt, J. Jeggle, J. Stenhammar, and R. Wittkowski, Pair-distribution function of active Brownian spheres in three spatial dimensions: Simulation results and analytical representation, Soft Matter **20**, 224 (2024).

[66] S. Bröker, M. te Vrugt, and R. Wittkowski, Collective dynamics and pair-distribution function of active Brownian ellipsoids in two spatial dimensions, Commun. Phys. **7**, 238 (2024).

[67] J. Jeggle, J. Stenhammar, and R. Wittkowski, Pair-distribution function of active Brownian spheres in two spatial dimensions: Simulation results and analytic representation, J. Chem. Phys. **152**, 194903 (2020).

[68] U. Marini Bettolo Marconi and P. Tarazona, Dynamic density functional theory of fluids, J. Chem. Phys. **110**, 8032 (1999).

[69] A. J. Archer and R. Evans, Dynamical density functional theory and its application to spinodal decomposition, J. Chem. Phys. **121**, 4246 (2004).

[70] A. J. M. Yang, P. D. Fleming, and J. H. Gibbs, Molecular theory of surface tension, J. Chem. Phys. **64**, 3732 (1976).

[71] J. Toner and Y. Tu, Long-range order in a two-dimensional dynamical XY model: How birds fly together, Phys. Rev. Lett. **75**, 4326 (1995).

[72] M. P. Holl, A. J. Archer, and U. Thiele, Efficient calculation of phase coexistence and phase diagrams: Application to a binary phase-field crystal model, J. Phys. Condens. Matter **33**, 115401 (2021).

[73] The constant α allows one to easily switch between common parametrizations.

[74] M. E. Cates and J. Tailleur, When are active Brownian particles and run-and-tumble particles equivalent? Consequences for motility-induced phase separation, Europhys. Lett. **101**, 20010 (2013).

[75] T. Frohoff-Hülsmann and U. Thiele, Nonreciprocal Cahn-Hilliard model emerges as a universal amplitude equation, Phys. Rev. Lett. **131**, 107201 (2023).

[76] U. Thiele, T. Frohoff-Hülsmann, S. Engelnkemper, E. Knobloch, and A. J. Archer, First order phase transitions and the thermodynamic limit, New J. Phys. **21**, 123021 (2019).

[77] H. Xu, Y. Huang, R. Zhang, and Y. Wu, Autonomous waves and global motion modes in living active solids, Nat. Phys. **19**, 46 (2023).

[78] T. H. Tan, A. Mietke, J. Li, Y. Chen, H. Higinbotham, P. J. Foster, S. Gokhale, J. Dunkel, and N. Fakhri, Odd dynamics of living chiral crystals, Nature (London) **607**, 287 (2022).

[79] J. Yan, S. C. Bae, and S. Granick, Rotating crystals of magnetic Janus colloids, Soft Matter **11**, 147 (2015).

[80] M. N. van der Linden, L. C. Alexander, D. G. A. L. Aarts, and O. Dauchot, Interrupted motility induced phase separation in aligning active colloids, Phys. Rev. Lett. **123**, 098001 (2019).

[81] N. H. P. Nguyen, D. Klotsa, M. Engel, and S. C. Glotzer, Emergent collective phenomena in a mixture of hard shapes through active rotation, Phys. Rev. Lett. **112**, 075701 (2014).

[82] Z. T. Liu, Y. Shi, Y. Zhao, H. Chaté, X.-q. Shi, and T. H. Zhang, Activity waves and freestanding vortices in populations of subcritical Quincke rollers, Proc. Natl. Acad. Sci. U.S.A. **118**, e2104724118 (2021).

[83] B. V. Hokmabad, A. Nishide, P. Ramesh, C. Krüger, and C. C. Maass, Spontaneously rotating clusters of active droplets, Soft Matter **18**, 2731 (2022).

[84] A. S. Moskalenko, A. W. Liehr, and H. G. Purwins, Rotational bifurcation of localized dissipative structures, Europhys. Lett. **63**, 361 (2003).

[85] J. Burke and E. Knobloch, Localized states in the generalized Swift-Hohenberg equation, Phys. Rev. E **73**, 056211 (2006).

[86] E. Knobloch, Localized structures and front propagation in systems with a conservation law, IMA J. Appl. Math. **81**, 457 (2016).

[87] At mean densities higher than $\bar{\phi} = -0.45$, one finds a larger $R_{\min} \approx 18.8$ due to the softening of the interface between uniform background and pattern. The interface is quite sharp at low T but widens at larger T.

[88] That their simulations do not show traveling crystallites may be due to their choice of boundary conditions.

[89] Z. F. Huang, A. M. Menzel, and H. Löwen, Dynamical crystallites of active chiral particles, Phys. Rev. Lett. **125**, 218002 (2020).

[90] M. P. Holl, A. B. Steinberg, M. te Vrugt, and U. Thiele, Data supplement for "Motility-induced crystallization and rotating crystallites", Zenodo, 2025, 10.5281/zenodo.17104279.